CONF-890145--26

UCRL--100420

DE89 015731

Flow, Heat Transfer, and Wavefront Distortion in a Gas Cooled Disk Amplifier

G. Albrecht
S. Sutton
H. Robey
B. Freitas

This paper was prepared for submittal to
SPIE OE LASE '89
Los Angeles, California
January 16-20, 1989

January 1989

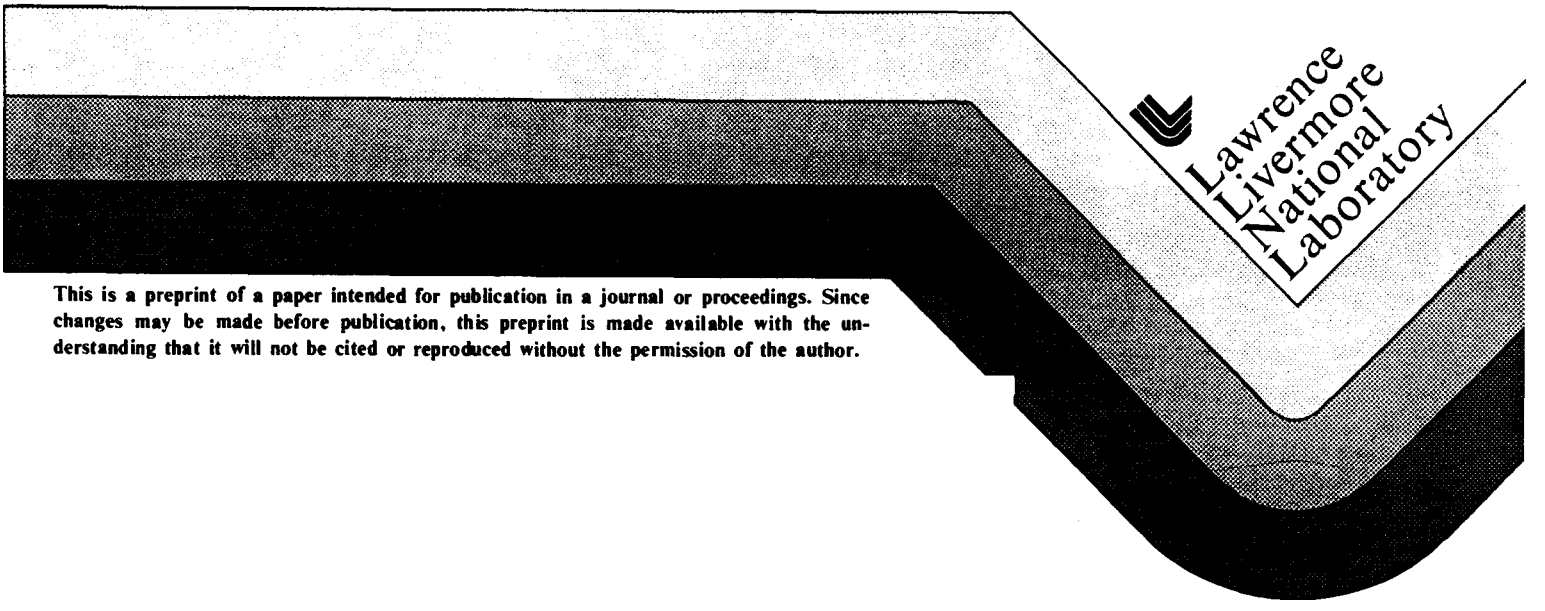

Flow, Heat Transfer, and Wavefront Distortion in a Gas Cooled Disk Amplifier*

G. F. Albrecht, S. B. Sutton, H. F. Robey, B. L. Freitas

University of California, Lawrence Livermore National Laboratory
P.O. Box 5508, L-487, Livermore, California 94550

ABSTRACT

The potential of the gas cooled disk architecture to operate at kilowatt to megawatt levels of average power is explored. The key issues investigated are flow and heat transfer in the cooling channel, the power required to perform the cooling and its implications for overall system efficiency, flow conditioning in the drift region, losses due to turbulent scattering, and beam quality due to optical distortions. In all cases an understanding of the issues leads to ways to mitigate or eliminate deleterious effects. Our conclusion is that the gas cooled disk geometry is an architecture which can lead to devices which are capable of average power levels reaching from a few kilowatts up to hundreds of kilowatts per beam line without stressing existing engineering or technology.

1. INTRODUCTION

Recent years have seen a strong resurgence of interest in high average power solid state lasers, which led to a large number of publications in the field.[1-3] The goal is lasers capable of output powers in the kilowatt vicinity with good beam quality and, for some applications, sufficient peak power to allow efficient frequency conversion. The thermo-mechanical issues and the resulting optical consequences which have to be overcome in this technology are generally familiar but are briefly reiterated for completeness. Figure 1a shows the distortions experienced in a classical rod geometry. Volume heating and surface cooling establish radial gradients which are sampled by the transmitted beam in such a way that focusing and a complicated form of depolarization take place. If one employs a slab type geometry (Fig. 1b), similar gradients occur but now in such a way that, to first order, rays traverse the gradients in a manner that a cancellation of distortions becomes possible. Several geometrical embodiments of these principles have been pursued to various degrees. The most attention to date has been given to the zig-zag geometry (Fig. 1c) where averaging occurs due to the beam zig-zagging between the plate faces as it travels down the gain medium. The second approach pursued at Lawrence Livermore National Laboratory was the gas cooled disk amplifier (Fig. 1d), where a series of disks are oriented under Brewster's angle, and averaging takes place during a single traverse through the plate by

*Work performed by the Lawrence Livermore National Laboratory under the auspices of the U.S. Department of Energy Contract W-7405-Eng-48.

virtue of its orientation with respect to the beam. A third approach which was investigated by the Laboratory for Laser Energetics at the University of Rochester is the active mirror where the beam reflects off the rear surface of a disk double passing the gain medium.[4,5] The present paper discusses key issues important to assess the potential of the gas cooled disk amplifier for generating large amounts of average power from a solid state laser.

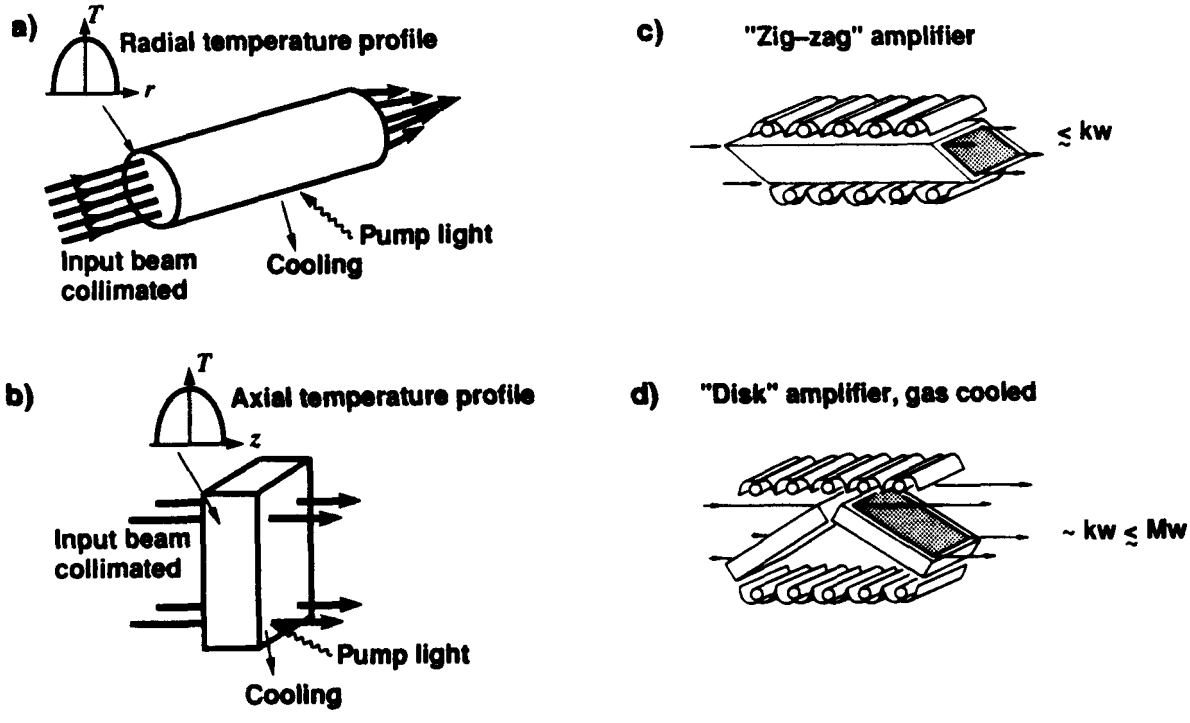

Figure 1. The left part of the sketch illustrates the basic problem of thermo-mechanical distortions degrading the beam quality if the resulting gradients are not sampled in such a way that a cancellation of distortions occurs. In rod geometries, radial gradients lead to severe beam distortions in average power systems. In slab geometries, the gradient can be oriented such that all rays sample the same gradients so that no beam distortion across the aperture results. The right portion depicts two possible embodiments of a slab type geometry. In the zig-zag laser, the beam repeatedly reflects off the pump faces as it travels along the gain medium; in the gas cooled slab a series of plates are oriented under Brewster's angle and cooled with a gas flowing across the surfaces.

A study in 1984[6] identified the gas cooled disk amplifier as an architecture which has the potential to scale solid state average power beyond the kilowatt towards the megawatt level. The paper also outlined some basic features of the geometry and indicated a variety of essential issues in need of further study. Figure 2 shows the basic geometry which is that of a disk amplifier[7] but with a cooling system added so that the device can be operated at average power. The

active medium disk is oriented under Brewster's angle. The cooling gas flows over the surfaces to remove heat across the thinnest dimension and from the largest faces, a prerequisite for all solid state average power architectures. As the beam propagates through the device, it also traverses the region between sets of Brewster plates which we call the drift region. There too, the gas flow has to be judiciously controlled to minimize beam distortion. Even though the refractive index of a gas is close to unity, the optical path length in the drift region is long enough so that changes in the path length integral across the aperture can amount to considerable phase variations across the beam. This will be discussed in more detail later.

There are two features intrinsic to the geometry which give it the potential for good beam quality. Firstly, the beam samples the laser slabs in such a way that mechanical distortions of this plate are seen in transmission rather than reflection as is the case in the zig-zag and active mirror architectures. Consequently, a given amount of geometrical distortion translates to a significantly smaller amount of beam distortion. Secondly, in the gas cooled disk amplifier geometry, the beam enters and leaves the gain medium through the large faces. In this way the beam does not sample any pump, stress, or temperature transition regions. Such transition regions still exist, of course, but we now have the possibility to locate them outside of the aperture which the beam has to traverse. On the other hand, the architecture demands that the beam traverses through the cooling medium. Because of this, gas is a logical choice. Thermo-optical distortions in a liquid would be orders of magnitude larger and therefore would dominate beam distortions. This issue obviously needs to be thoroughly understood and will be treated in detail below.

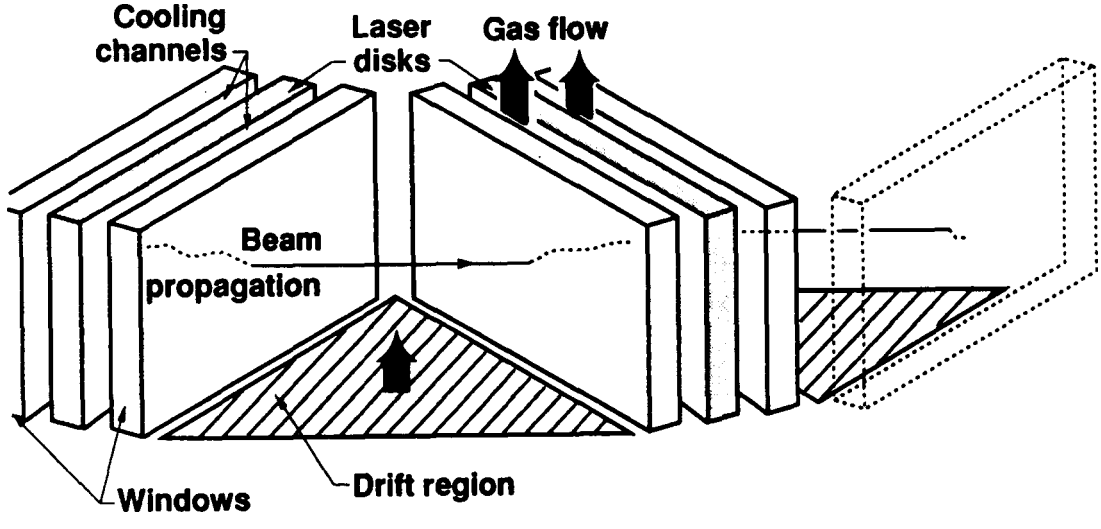

Figure 2. The essential geometry of a gas cooled disk amplifier shown in more detail. The disks are cooled by a gas flow across the surfaces which is confined by windows. Gas also flows through the drift region space to make sure that buoyant recirculation will not destroy the beam profile in the regions between disk assemblies.

The gas cooled disk geometry scales to large average powers since the device aperture can be increased without changing the thickness of the plate across which the heat is removed. By way of a simple illustration, consider a single disk in an amplifier operated at a conservative fluence of 10 J/cm^2 and a repetition rate of 10 Hz. Such very common values correspond to a power density of 1 MW/m^2. It is, of course, not just one disk but all disks in the amplifier which contribute to this fluence, and it is also through the total surface area of all disks that the heat is being removed. In fact, for a postulated 50% extraction efficiency, one finds the surface heat flux Q to be:

$$Q = (\chi/\#\ \text{of disks}) \bullet \text{power density} \qquad (1)$$

for $\chi = 1$ (for X Joules of energy stored in the inversion, $\chi \bullet X$ Joules of waste heat must be removed) and for 30 disks we get a surface heat flux of 3 W/cm^2. Such a crude estimate illustrates that even for conservative operating parameters, MW/cm^2 of average power flux and very benign surface heat fluxes are obtained. The paper following this one (High Average Power Gas Cooled Brewster Slab Lasers: Power Scaling Laws and Material Requirements) provides design examples based on more detailed calculations, the resulting values for average power density and surface heat flux will be of much the same order.

2. KEY PHYSICS AND SCALING ISSUES

To judge the likelihood of a successful development of this architecture, one has to understand five basic issues which are key to its practical feasibility. These are:

The flow characteristics of the cooling gas and how it transfers heat from the hot laser disk.

The power requirement to perform this cooling and how it impacts device efficiency.

The distortion of transmissive optics which comes in contact with the cooling gas.

The losses and distortions which the beam experiences when it travels through the turbulent gas flow in the cooling channels.

The flow conditioning in the drift regions which has to minimize beam distortions while preserving the top and bottom plates as high quality reflectors for pump light.

In the following we outline the computational and experimental work we have undertaken to clarify these points and how they establish the feasibility of the gas cooled disk architecture. In this paper we give a broad overview of some of the work done so far. Detailed discussions of individual studies will appear in a series of papers which are being written at this time. Scaling laws and an outline of actual systems will be discussed in the next paper in this session.

2.1 Turbulent flow and heat transfer

Figure 3 shows in more detail the essential elements of the flow channel. The gas passes from the supply line through the acoustic isolator into the upstream nozzle area. The acoustic isolator prevents pressure pulses generated in the compressor and supply line from entering the channel; it effectively sets up a new initial condition for the flow. The nozzle then accelerates the flow into the channel to speeds of order Mach 0.1. This number is essentially a compromise between a high enough flow speed to produce sufficient mass flow for cooling and a low enough flow speed to limit compressor power requirements to tolerable levels. The nozzle furthermore must accelerate the flow uniformly without instabilities occurring at the nozzle walls. As the accelerated flow enters the channel proper, it encounters a trip which helps define the origin of the developing boundary layers. These boundary layers grow from either side and eventually merge in the channel center. A little further downstream the velocity across the channel thickness will have reached a fully developed profile, i.e., its shape will remain constant down the channel. The process just described is referred to as the viscous conditioning of the flow.

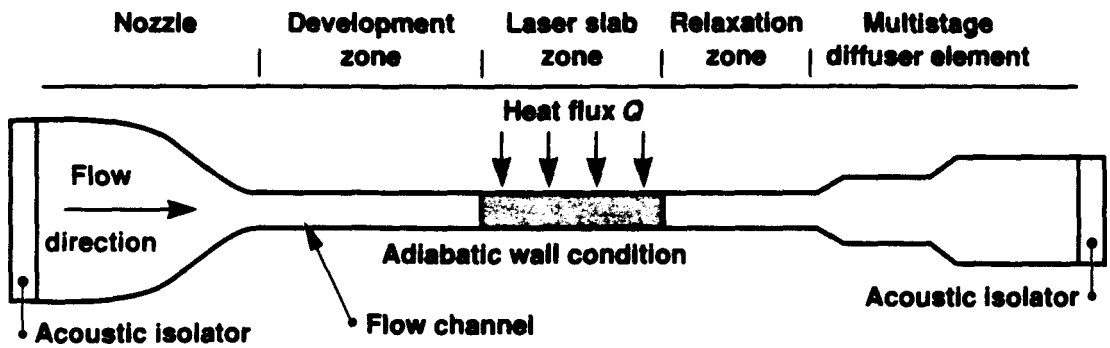

Figure 3. A schematic representation of a cooling channel showing inlet nozzle, the flow channel proper with the laser slab where heat is removed by the fluid, a relaxation region, and a diffuser.

Once viscous conditioning is complete, the flow enters the channel section where it encounters the heated laser disk. Now a thermal boundary layer will develop, quite analogous to the viscous development just described. Particularly during the early stages of this development phase, heat transfer characteristics vary dramatically. Once the thermal boundary layer is fully developed, the shape of the temperature profile across the channel will not change anymore. It is essential that this development be complete before the gas encounters the laser disk since the streamwise temperature gradients in the developing thermal boundary layer are steep and highly nonuniform. To accomplish this, one has to provide for a preheat zone upstream of the actual disk where this boundary layer development can occur. Since it is across this fully developed thermal boundary layer profile that heat is removed from the slab, its characteristics and heat transfer capabilities are of pivotal

importance in determining under what flow and optical conditions how much surface heat flux can be removed under acceptable optical conditions.

After the disk, the gas passes over a relaxation zone so that downstream effects will not influence the gas flowing over the disk. Next the gas enters a diffuser where the gas kinetic energy is reconverted to stagnation pressure. This has to be done with the highest possible efficiency since the stagnation pressure drop from nozzle entrance to diffuser exit is directly proportional to the required compressor power. A pictorial view of some of these effects is given in Fig. 4. It illustrates the development of the velocity, temperature, and density profile along the channel. Note that the velocity profile is not influenced by the heat removal process. Also note how the formation of a thermal boundary layer with its steep thermal gradients at the disk surface severely modifies the temperature and density profile near the hot wall.

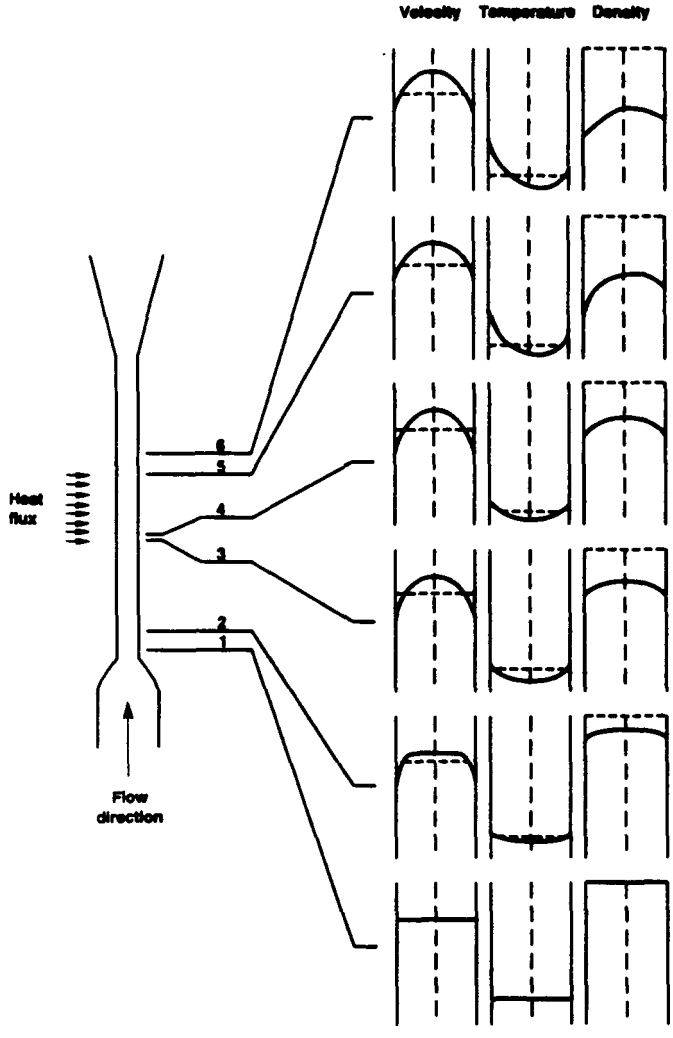

Figure 4. Diagram of flow development in the channel. Shown are the velocity, temperature, and density profiles. The velocity profile starts out as a uniform flow which gradually turns into the typical channel flow profile. It is little changed by the heat removal process. Note the acceleration of the core of the flow. The temperature profile initially shows only the frictional wall temperature rise. As heat is removed from the laser slab, the gas temperature close to the surface rises steeply due to formation of a thermal boundary layer.

Figure 5 shows, based on a simple energy balance equation, how much surface heat flux can be removed versus Mach number for a variety of conditions. Also indicated are various processes which eventually limit the plot space. As the surface heat flux increases, either the temperature gradients get so steep that thermo-mechanical stresses eventually break the disk or the gain medium simply gets hot enough to reduce gain through a variety of mechanisms. Straight lines through the origin are lines of constant pressure. As the pressure increases, it is obviously possible to remove the same surface heat flux at ever lower Mach numbers. At some point, however, engineering considerations will limit the maximum operating pressure. This limits access to the northwest quadrant of the plot. Higher Mach numbers are excluded since the compressor power needed to drive the gas around scales with the third power of the Mach number. This in turn has eventually unacceptable consequences for the overall system efficiency. Also shown is the area occupied by systems optimized with respect to maximum power output and minimum cooling requirements as a function of system aperture. It illustrates very clearly one of the most benign scaling laws of the gas cooled architecture: larger systems, despite providing more output power, are increasingly easier to cool.

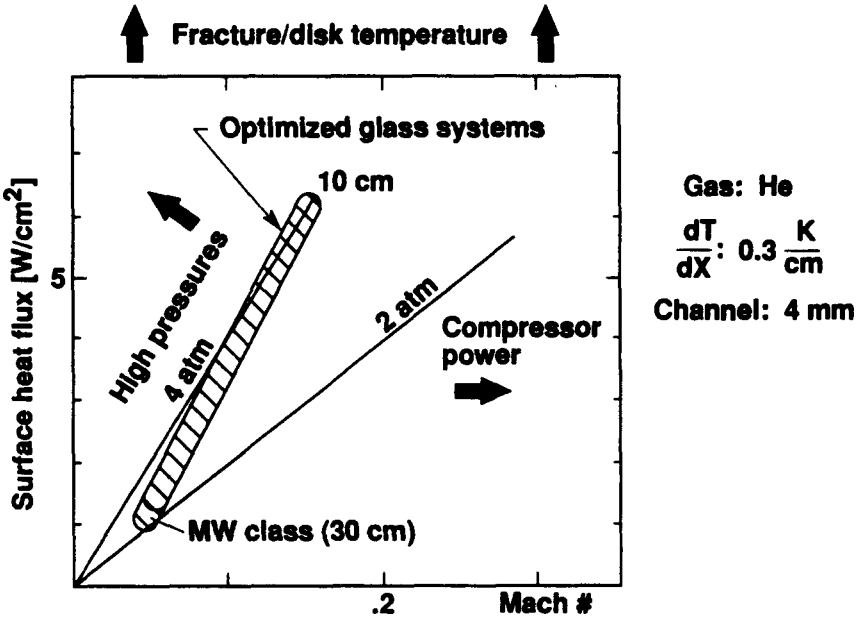

Figure 5. The plot shows the surface heat flux that can be removed versus Mach number for different pressures. Also shown are the locations of systems which are optimized with respect to maximum lasing output and minimum cooling requirements. Note that the occurring heat fluxes DEcrease with system aperture and MW class systems occupy a more benign region of this design space than smaller devices.

Figures 6 and 7 show two results which compare computed details of the flow behavior to the experiment. The first plot shows how the

static pressure drops as the gas first squeezes through the nozzle, flows down the channel, and how much stagnation pressure is recovered in the diffuser. The slight downward curvature in the channel section is due to self acceleration. As the gas proceeds down the channel, viscous friction at the walls will dissipate some of the flow's energy which will manifest itself as a drop in static pressure down the channel. Simultaneously, as more and more of the gas is decelerated at the channel walls, mass conservation will force the core of the flow to accelerate beyond the core velocity at the channel entrance. This effect becomes particularly severe at higher Mach numbers and eventually leads to choking if the channel is long enough for a given entrance Mach number. The solid line in the plot is a computation assuming isentropic flow through the nozzle and Fanno flow through the channel. The second plot shows the temperature profile across the channel thickness for a surface heat flux of 3 W/cm^2 and a Mach number of 0.3. The experimental points were obtained with a micro thermistor probe and deconvoluted for flow stagnation and thermal conduction at the probe surface. The temperature at the slab surface itself was measured with a calibrated thermal imaging camera. The solid line is a computation using the TEXSTAN[8] flow code which solves the boundary layer form of the Navier-Stokes equations with a two-equation closure model to describe turbulence. The turbulence is characterized in terms of a turbulent kinetic energy and the mean rate of dissipation. Near-wall effects are included through additional damping terms. As both plots show, the agreement is good. Numerous such comparisons have provided us with accurate tools for predicting flow behavior in the cooling channels.

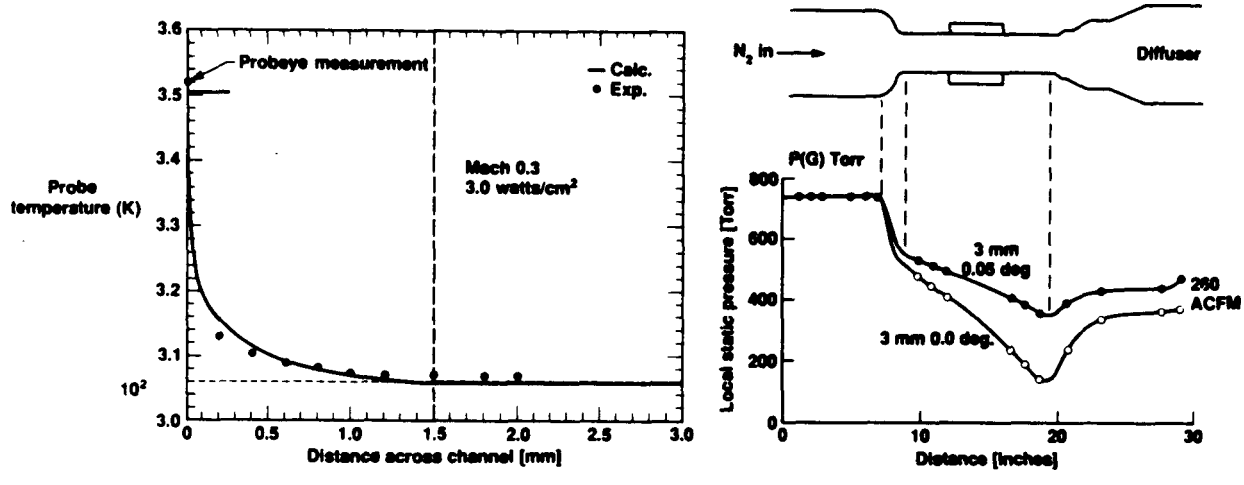

Figures 6 & 7 The left figure shows how the static pressure drops as the gas goes through the nozzle, down the channel, and through the three stage diffuser (dots = experiment, line = calculation). The right figure shows a comparison between calculated (solid line) and measured (dots) temperature profile across the channel for a surface heat flux of 3 W/cm^2 and a flow velocity of Mach .3.

2.2 Turbulent scattering in the flow channels

For efficient extraction, high gain-to-loss ratios are desirable. In gas cooled disk amplifiers, a new loss mechanism is given by scattering of the beam from the turbulent refractive index variations in the gas flow. To investigate this turbulent scattering, we set up a simple Schlieren experiment, suitably modified to also show the intensity distribution in the focal plane and to measure the fraction of intensity which was scattered. Figure 8 shows representative Schlieren pictures of the flow at Mach 0.2 with (5 W/cm^2) and without removing heat. It is clear that the heat removal process greatly increases the scattering. Note the beautiful development of the thermal boundary layer visible through increased scattering. It is also instructive to photograph the intensity distribution in the focal plane. To block out the very much brighter diffraction pattern from the flow window aperture, we insert a cross-shaped mask which covers ±6 diffraction orders on either side from the center line to make the faint scattered light visible. Figure 9 shows the result for cold flow at Mach .6 and the background for comparison. Since the experimental parameters are known, one can make explicit statements about the characteristics of the average scatter in the turbulent flow. It has an elliptical shape with an eccentricity which increases with increasing flow speed, reaching about 2:1 at Mach .6 ,its long axis is aligned with the flow direction. At Mach .6 it is about 1.1 mm long and .7 mm diameter which is about 1/5 of the channel thickness.

M = .2
Q = O W/cm²
(essentially background)

M = .2
Q = 5 W/cm²

Figure 8. On the left is a Schlieren picture at Mach .2, 0 W/cm^2 (essentially background); on the right is Mach .2, 5 W/cm^2. Note how the development of the thermal boundary layer manifests itself trough increased scattering from temperature fluctuations.

Figure 9 also suggests an obvious way to measure the fraction of scattered light. The light passing the mask is collected on a large area photo detector, corrected for the amount covered by the mask,

and ratioed to the light incident on the flow channel. Figure 10 plots the fraction of scattered light versus the 4th power of the Mach number. Given practical surface heat fluxes and channel thicknesses, together with reasonable compressor powers, the envisioned operating regime for a gas cooled disk amplifier will certainly not exceed Mach .3. For these Mach numbers the turbulent scattering in cold flow is well below .1% for N_2 in a typical flow channel. Figure 11 shows to what extent heat removal enhances turbulent scattering. At 4 W/cm^2 and Mach .3, enhancements of about a factor 3 are observed. If He is used, the scattering will be lower by a factor $(n-1)^2$ plus the entire system can be operated at lower pressures, which has obvious engineering advantages and further reduces turbulent scattering. Taken altogether, He is the preferred gas and will make turbulent scattering a complete non-issue.

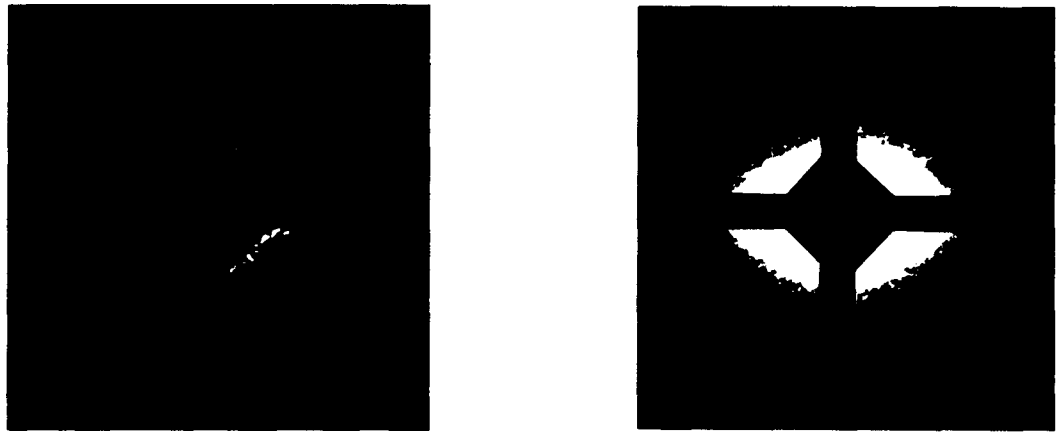

Figure 9. The intensity distribution in the focal spot. On the left is the background, on the right a flow at Mach 0.6 with no heat removal.

2.3 Flow conditioning in the drift region

As was pointed out in the discussion of Figure 2, the flow in the space between the slab assemblies must also be conditioned for minimal beam distortion. To simply trap gas will establish buoyancy driven recirculation cells with refractive index scale lengths of order of the beam diameter. This would be about the worst possible scenario for beam distortions. To evacuate this space would require impracticably thick flow separation windows to hold the flow channel pressure without bending the windows. One also needs to keep in mind that the top and bottom plates, through which any gas flow must exit and enter, must serve as high quality pump light reflectors while simultaneously serving to enter and exit the gas. In discussing turbulent scattering in the flow channel, we distinguished strongly Mach number dependent scattering in the absence of surface heat flux and scattering from temperature fluctuations which occur in the presence of surface heat flux. The bulk flow velocity of drift region gas is so low that, once buoyant recirculation is overcome,

scattering levels should essentially depend on temperature effects only. The biggest thermal effect will be the temperature distribution across the reflector plate because it is subjected to average power pump light. This temperature distribution will be imparted to the gas as it enters the drift region. It is these large scale gradients which the turbulence must break up and randomize close to the reflector surface.

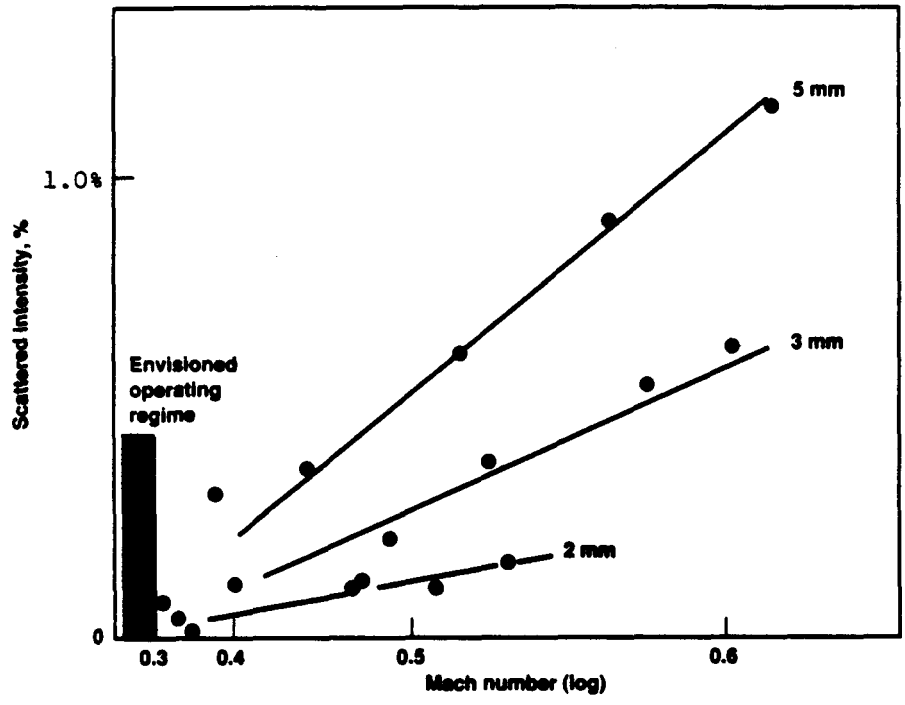

Figure 10. Fraction of scattered intensity versus Mach number. Scattering scales as the 4th power of the Mach number and about the 3/2 th power of the channel thickness.

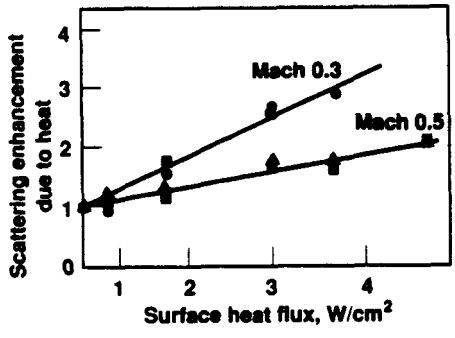

Figure 11. Surface heat removal is enhanced due to scattering from temperature fluctuations. Slower flows get hotter and therefore scatter more.

After several iterations we arrived at a flow geometry indicated in Fig. 12. The gas enters through a series of fine jet slots arranged perpendicular to the beam direction. The slots are fine enough to keep the plate solidity above 98%. Since the slots are continuous, there is no structure on the flow transverse to the beam. Furthermore, this arrangement causes a high rate of entrainment of the gas between the jets which leads to a high turbulent intensity in the background gas. This, in turn, leads to

rapid small scale mixing of scalar gradients in the drift region which will cause some scattering of the beam, but ensures the absence of large scale gradients which would cause incorrigible distortions. The diagnostic used to experimentally investigate these effects is essentially identical to that used to understand turbulent scattering in the flow channel. To simulate a temperature gradient across the reflector surface we simply installed a heater in the center of the drift region. A Schlieren picture of the drift region with the beam passing perpendicular to the jet slots is devoid of any flow features even at exposure levels where optical imperfections start to flood the background. This is good news, of course, but gives no insight in the prevalent mechanisms. Hence we produced a Schlieren picture of the jet slots when viewed side on, that is along the direction of the slot (Fig. 13). The picture clearly shows that, for flow rates of interest, a coherent jet structure is essentially absent and extremely rapid mixing takes place very close to where the jet enters the drift region space. This was not the case for round jets. If one attempts to make the drift-region-equivalent picture of Fig. 9, one finds that the scattering angle is too small for scattered light to extend significantly beyond a mask size which still covers the brightest orders of the diffraction pattern. This limits the feature size mainly responsible for the scattering to around 1 cm, which compares well to the jet slot spacing. A similar scale length is found when one performs a correlation experiment with two hotwire probes. Furthermore, these findings are consistent with the theoretical picture that turbulent energy is fed in the system at the largest relevant geometrical scale and cascades towards smaller sizes from then on. Figure 14 shows the fraction of light scattered. Firstly, it is clear that this fraction depends only weakly on the flow speed; secondly, the scattered fractions are seen to be of order 10^{-3} unless fairly extreme temperature gradients are being considered. Also, since the calibration of the scattered amount is particularly difficult for these small scattering angles, the vertical axis values are uncertain to within about a factor two. Again, if He is used, scattering levels fall well below levels where they need to be taken into account.

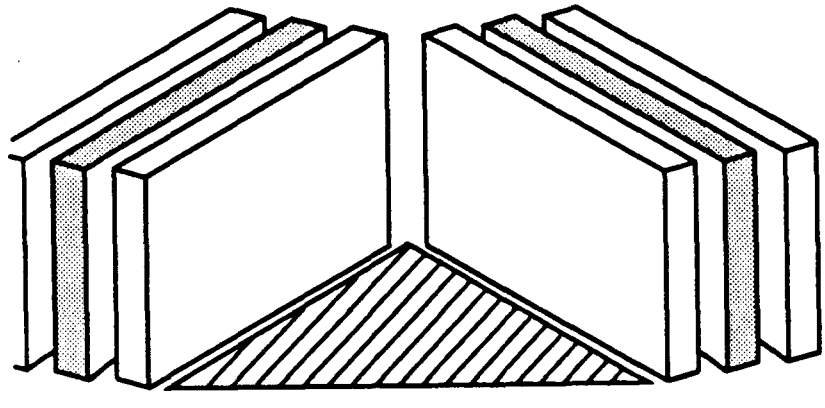

Figure 12. The drift region uses slow gas flow through jet slots to condition the flow between slab assemblies. This provides for high turbulent background intensities to break up large scale temperature gradients.

Figure 13. Side on (in the direction of the jet slots) view of the drift region jets shows how quickly they loose their coherent structure due to turbulent mixing.

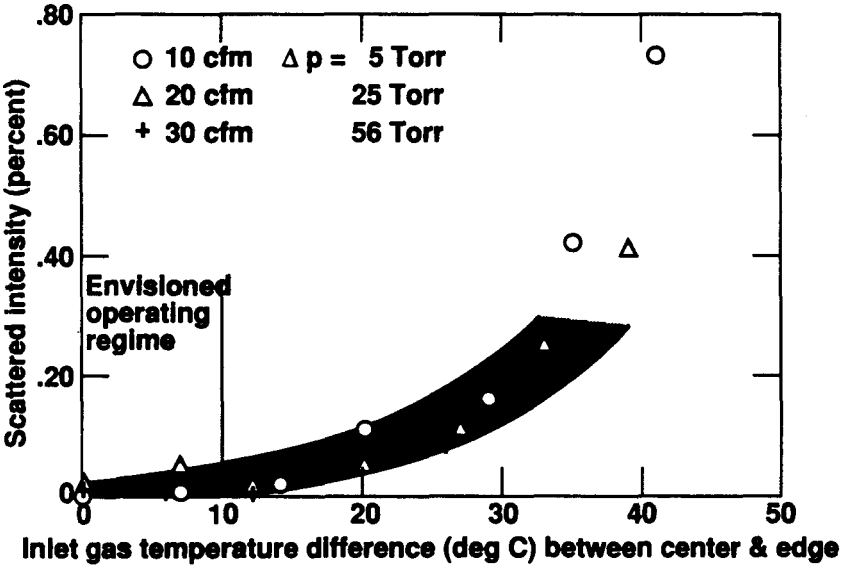

Figure 14. Drift region scattering levels as measured in air at atmospheric pressure versus center to edge temperature difference. Flow rates of 10 to 20 cfm are sufficient to suppress buoyant recirculation.

2.4 Compressor power requirement to perform cooling function

The power needed to drive the gas through the cooling loop is composed from a number of contributions. First, one has to provide the necessary power to the preheat section to let the thermal boundary layer develop to its steady state profile before the flow encounters the slab. Then the frictional dissipation of bulk

momentum at the channel walls and in the diffuser constitutes a drag which has to be overcome. Finally, the drift region flow must be powered as well. We describe the problem by defining the efficiency of a single shot system (no cooling power needed) to be eff(SS), and the efficiency of this same system, now operating under average power, as eff(AP). Hence the system efficiency decrement

$$SED = [eff(SS) - eff(AP)] / eff(SS) \quad (2)$$

is small if the efficiency under average power is almost equal to the single shot efficiency. Solving for eff(AP) shows that a 10% system efficiency decrement, for example, means that a system which is 5% efficient under single shot conditions has its efficiency reduced to 4.5% under average power conditions. The basic strategy of describing this efficiency problem is to set up a closed system of equations, so that the compressor power is expressed as a function of all relevant parameters. Some of these, like the streamwise temperature gradient, are limited by optical distortion considerations. Others, like the surface heat flux, are given by laser disk material parameters. After successive elimination of unknowns, differentiation with respect to the remaining variable then allows one to find, for given inputs, the minimum possible compressor power which fulfills all other requirements. Figure 15 summarizes the results by plotting the system efficiency decrement versus system aperture for operation at a thermal shock of .5 W/cm, a streamwise temperature gradient of .3 K/cm and a χ of 2. Only systems which are optimized with respect to ASE and slab fracture are considered. Small aperture systems of high aspect ratio will run at high surface heat flux and hence require higher Mach numbers and thicker channels (and therefore more compressor power) than their large aperture counterparts, even though the disk is smaller. Large apertures, however, produce considerably more average power than smaller slabs. These circumstances conspire to drop the system efficiency decrement as shown in the plot. Nevertheless, the efficiency decrement stays well below 20% even under the most stressing conditions.

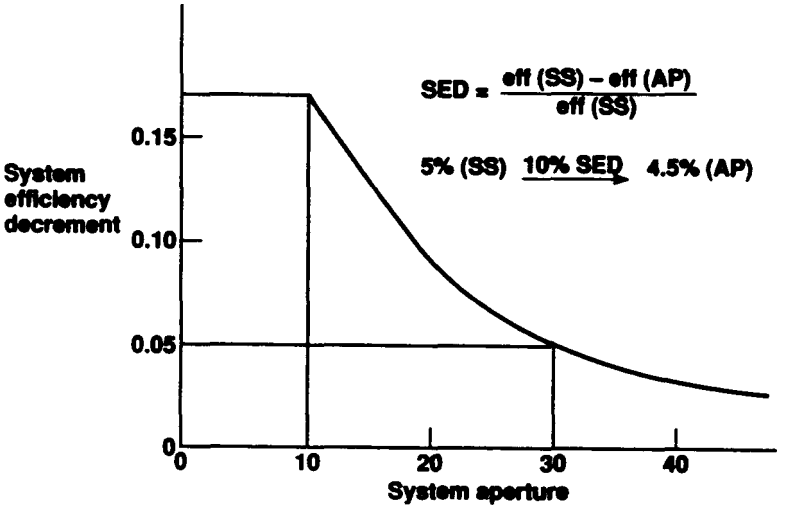

Figure 15. The system efficiency decrement (explained in text) decreases as the system aperture increases because a decreasing amount of cooling power is compared to an increasing amount of laser output.

Figure 16 shows the different contributions to the total cooling power for selected apertures. The ratio of drag to preheat power requirement stays roughly constant. The power needed to drive the drift region gas becomes a gradually larger fraction of the total power required to cool.

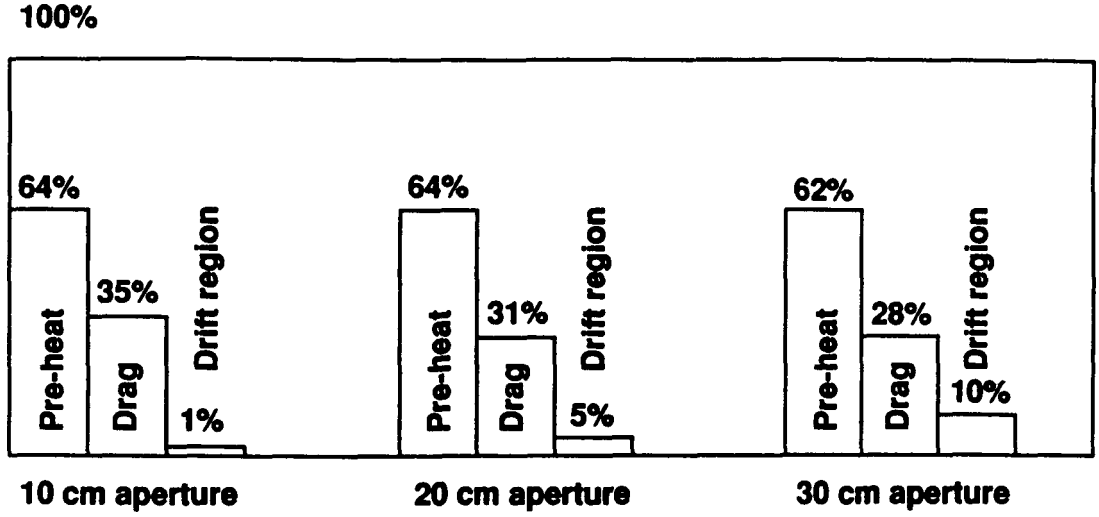

Figure 16. The total cooling power is shared between the preheat power needed to form the thermal boundary layer, to overcome drag and to drive the drift region. For increased system aperture, the drift region power requirement increases somewhat at the expense of preheat and drag power requirements.

2.5 Beam distortion due to optical elements

As was discussed above for the flow channel, the gas pressure decreases in the flow direction because of viscous drag in the walls. Since the gas removes heat in the process, it also gets increasingly hotter as it flows down the channel. On the drift region side, however, pressure and temperature are essentially constant with height. Hence the flow separation windows are subjected to a temperature and pressure gradient through their thickness which changes with height. This will give rise to geometrical distortions which in turn will distort the beam going through these windows. Here we will briefly outline the results of a study investigating this problem.

For a window of thickness d and refractive index n, placed perpendicular to the beam, the optical path length difference from the undeformed case is given by:

$$OPD = nd/2n^2 \cdot [(df/dx)^2 + (df/dy)^2] \qquad (3)$$

where the shape of the deformed surface is described by a function $f(x,y)$. If this plate is rotated under Brewster's angle, the resulting OPD takes the form:

$$OPD = \frac{nd}{\sin\varphi_B}\left[1 - \frac{1}{n^3}\frac{\partial f}{\partial y} + \frac{1}{2n^4}\left(\frac{\partial f}{\partial x}\right)^2 + \frac{1}{2n^2}\left(\frac{1}{n^2} - 1\right)\left(\frac{\partial f}{\partial y}\right)^2\right] \qquad (4)$$

Viewing the OPD contours as fringes in an interferometer originally set to zero fringe, one can see that the fringe pattern in (3) is essentially preserved in (4), but the axes are now stretched by different factors in the x and y direction. Note that the tilt also introduces a term linear in df/dy. To see its significance, recall that the surface deformations described by f(x,y) are caused by temperature differences ΔT through the window and the resulting thermal expansion $\alpha \cdot \Delta T$. Pressure differences ΔP cause surface deformations proportional to $Ar^3 \cdot \Delta P/E$ where Ar is the window aspect ratio (width to thickness) and E is Young's modulus. For typical pressure and temperature differences, these factors are at most of order 10^{-4}. From these considerations, it is clear that the linear term in (4), associated with the rotation of the deformed window towards Brewster's angle, contributes the most fringes. A cooled slab, however, requires <u>two</u> windows, one on each side. At the other window, the surface distortions are the same but of opposite direction. Hence one simply needs to offset the two windows by the same amount the beam is offset as it traverses the assembly and f(x,y) in the first window will equal -f(x,y) in the second window. If two windows are positioned in this particular manner, we refer to them as a conjugate window pair. This leads to a cancellation of the linear df/dy term and the combined OPD for two windows contains only terms of order $\left(\frac{\partial f}{\partial x}\right)^2$ and $\left(\frac{\partial f}{\partial y}\right)^2$.

The smallness of the $\alpha \cdot \Delta T$ and $Ar^3\ \Delta P/E$ factors makes OPD (2 windows) to be at most of order 10^{-3} fringes per slab, depending on the size of the aperture and the materials involved. It is also due to the smallness of these factors that the effects of the end windows of the device, where the beam enters into the outside world, is negligible. The actual fringe distortion due to these end windows can be readily calculated using (3). A pictorial representation of these findings is given in Figs. 17 to 19. Figure 17 shows the geometrical distortions of a flow separation window due to a changing pressure and temperature on the flow channel side and a constant temperature and pressure on the drift region side. Figure 18 shows qualitatively the resulting fringe shape for a single window perpendicular to the beam or a conjugate window pair under Brewster's angle. Figure 19 indicates the fringe shape due to an end window with simply supported edges.

Apart from the window distortions just discussed, the slab and the windows get gradually warmer along the flow direction since the gas constantly removes heat from the disk. This gives them a slightly prismatic shape which deflects the beam. The typical magnitude of this deflection per slab assembly goes from a fraction of a fringe to a few fringes for apertures from 10 cm to 30 cm and typical operating parameters for surface heat flux, Mach number, and so on. In larger systems this beam deflection is easy to mitigate by counter-flowing, i.e., every five slab cluster.

From this study one concludes that despite complicated geometrical distortions of the flow separation windows, they can be arranged in such a manner that only simple beam pointing remains as the dominant optical distortion in a gas cooled disk amplifier. Even this beam pointing can then be cancelled by counter-flowing the gas in every other unit.

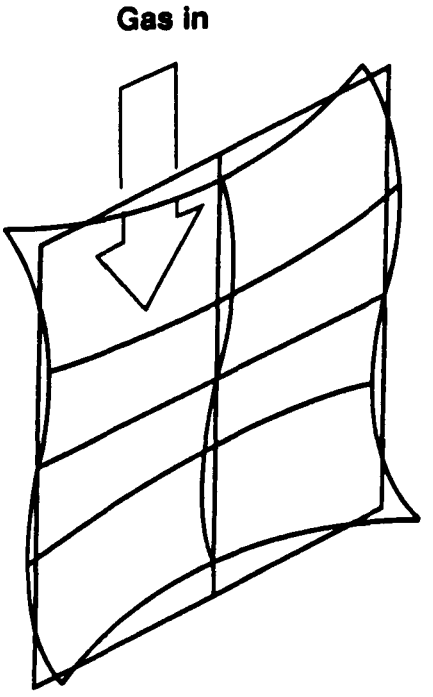

Figure 17. Representative shape of the geometrical distortion of a flow separation window in a gas cooled disk amplifier under heat removal conditions.

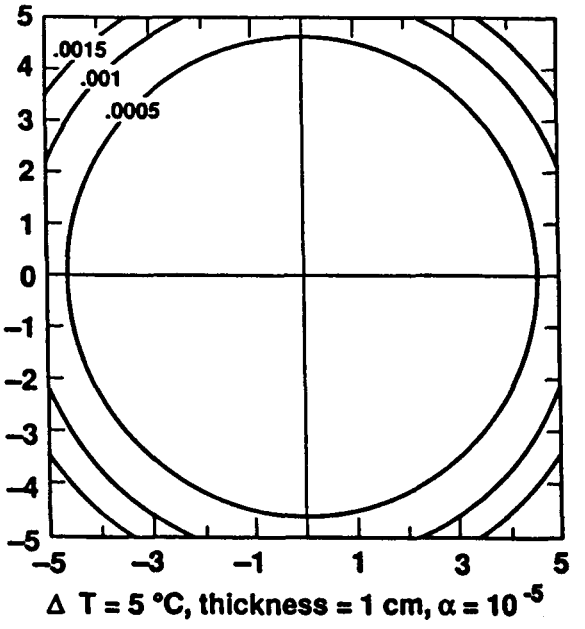

Figure 18. Remaining optical path difference contours of a disk assembly with two conjugate flow windows. The count across the aperture is of order 1/1000 of a fringe.

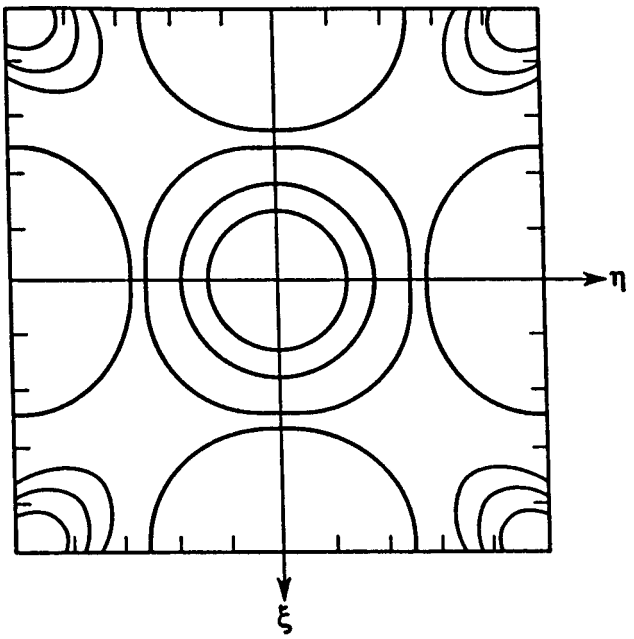

Figure 19. Representative shape of optical path difference contours of a simply supported end window under uniform pressure. For increasing thickness the fringe count across the aperture can be made arbitrarily small.

3. CONCLUSION

Over the past few years, the key issues deciding the practical feasibility of a gas cooled slab disk amplifier which can operate at average power have been favorably resolved. Heat transfer with turbulent gas flow can remove surface heat fluxes which are close to the disk fracture level without encountering unacceptable surface temperature gradients. The power requirements to perform the cooling function result in an efficiency decrement which, for the hottest and smallest systems, is well below 20% and for larger apertures is more of order 5%. The optical distortions in the flow separation windows can be, by proper construction, cancelled to 1st order so that simple beam pointing due to caloric heating is the dominant effect. Even this effect in turn can be cancelled by counter-flowing every other cluster. For practical system Mach numbers and if He is used as the coolant gas, turbulent scattering in the flow channel as well as the drift region becomes of an order lower than losses due to scattering of well polished surfaces. Our next effort should be the design and engineering of a gas cooled slab test amplifier section to show that all individual effects investigated so far will harmonize as anticipated.

4. ACKNOWLEDGMENTS

In the process of this work we had many worthwhile discussions with our colleague William Krupke. Al Erlandson performed scattering measurements on earlier versions of the drift region.

5. REFERENCES

1. See, e.g., Proc. SPIE Vols. 622 and 736 and the numerous references within the individual articles. Proceedings available from SPIE, P.O. Box 10, Bellingham, WA 98227-0010.

2. CLEO 1988 papers THP1 to THP4 and THV1 to THV4.

3. LLNL Medium Average Power Solid State Laser Tech. Info. Seminars, 1985 to 1988.

4. J. H. Kelly, et al., "High Repetition Rate Cr:Nd:GSGG Active Mirror Amplifier," Opt. Lett. 12, 996-998 (1987).

5. K. A. Cerqua, et al., "Strengthened phosphate glass in a high rep rate active mirror amplifier geometry," Appl. Opt. 27, 2567-2572 (1988).

6. J. L. Emmett, W. F. Krupke, W. R. Sooy, "The Potential of Average-Power Solid State Lasers, LLNL, UCRL 53571 (1984).

7. A comprehensive summary of disk amplifier physics is given in J. E. Murray, H. T. Powell, B. W. Woods, "Optimized Flashlamp Pumping of Disk Amplifiers," Proc. SPIE Vol. 609.

8. M. E. Crawford, W. M. Kays, "STAN5 - A program for numerical computation of 2D internal and external boundary layer flows. NASA CR-2742, Nov. 1976.